https://doi.org/10.3311/PPci.41892

Periodica Polytechnica Civil Engineering, 69(4), pp. 1203–1215, 2025

Comparative Assessment of Pore Structure and Water Retention in Concrete Using MIP, CT, SEM, and Dewpoint Techniques

Miklós Pap[1*], András Mahler[2], Zsombor Illés[2], Salem Georges Nehme[3], András Biró[3]

[1] Department of Hydraulic Engineering, Faculty of Water Sciences, Ludovika University of Public Service, Bajcsy-Zsilinszky u. 12–14., H-6500 Baja, Hungary
[2] Department of Engineering Geology and Geotechnics, Faculty of Civil Engineering, Budapest University of Technology and Economics, Műegyetem rkp. 3., H-1111 Budapest, Hungary
[3] Department of Construction Materials and Technologies, Faculty of Civil Engineering, Budapest University of Technology and Economics, Műegyetem rkp. 3., H-1111 Budapest, Hungary
[*] Corresponding author, e-mail: pap.miklos@uni-nke.hu

Received: 12 August 2025, Accepted: 04 September 2025, Published online: 06 October 2025

Abstract

Understanding water retention and pore structure in concrete is essential for modeling unsaturated flow and assessing long-term durability, particularly in containment and deep foundation structures. This study investigates two concrete mixtures with different water-to-cement (w/c) ratios (0.40 and 0.50) using a multi-method approach. Water retention curves (WRCs) were measured with a chilled-mirror dewpoint potentiometer and fitted using the Fredlund–Xing model. Pore structures were analyzed *via* mercury intrusion porosimetry (MIP), X-ray computed tomography (CT), and scanning electron microscopy (SEM). Results show that the mixture with the lower w/c ratio exhibits a higher proportion of fine pores, while the higher w/c ratio leads to a broader pore size distribution and a flatter WRC. MIP-based WRC estimations provided a rough approximation but consistently underestimated measured retention values. CT and SEM revealed distinct pore size domains, with pore size distributions fitting better to a lognormal model than to a Weibull distribution. Although each technique offers only partial insight, their combined application allows for a more comprehensive understanding of concrete's pore network and its effect on hydraulic behavior. The findings highlight both the potential and the limitations of using indirect pore structure data to estimate water retention characteristics in cementitious materials.

Keywords

concrete, porosity, pore size distribution, water retention curve

1 Introduction

Understanding fluid transport in porous building materials such as concrete and asphalt under saturated and unsaturated conditions is essential for lifespan analysis and advanced modeling. In practice, these materials are often partially saturated, with permeability varying dynamically during wetting–drying cycles. Even small reductions in moisture content can markedly decrease the hydraulic conductivity of unsaturated media, a relationship that can be quantified through the water retention curve (WRC) [1–3]. Although originally developed for unsaturated soils, theoretical models for WRC behavior have been successfully extended to other porous materials, including concrete [4–6], asphalt [7], and geotextiles [8].

For deep foundation elements such as diaphragm walls, watertightness is critical. Since complete impermeability cannot be achieved in concrete, WRC data are essential for predicting long-term water retention behavior, estimating permeability, and modeling seepage over time. Such insights are particularly vital for containment structures designed to store hazardous or radioactive waste, where water ingress and egress must be prevented [9]. Beyond containment, understanding water movement in concrete also informs durability assessments, particularly regarding reinforcement corrosion, where moisture content and degree of saturation are key controlling factors.

Cite this article as: Pap, M., Mahler, A., Illés, Z., Nehme, S. G., Biró, A. "Comparative Assessment of Pore Structure and Water Retention in Concrete Using MIP, CT, SEM, and Dewpoint Techniques", Periodica Polytechnica Civil Engineering, 69(4), pp. 1203–1215, 2025. https://doi.org/10.3311/PPci.41892

The pore structure and porosity of concrete directly influence water retention, yet the relationship between porosity determined by different techniques and WRC characteristics remains unclear. Common methods – mercury intrusion porosimetry (MIP), X-ray computed tomography (CT), and scanning electron microscopy (SEM) – differ in principles, resolution, and sampling scale [10–13]. MIP yields quantitative pore size distributions but may alter the microstructure due to high intrusion pressures and is less sensitive to large pores. CT provides 3D structural information but cannot resolve micropores [14], while SEM delivers high-resolution images of limited areas and requires destructive preparation [15].

Earlier comparative studies attempted to bridge this gap by linking pore structure characterization to moisture transport properties. For instance, while MIP-derived pore size distributions often correlate with the initial part of the WRC, discrepancies appear at higher saturation levels due to ink-bottle effects and limitations in resolving connected porosity [16]. CT-based analyses have been shown to capture larger pore features and crack networks that strongly influence permeability, yet their resolution constraints may underestimate fine-scale retention processes [17, 18]. SEM investigations have highlighted the importance of interfacial transition zones (ITZs) and microcracks, which can significantly alter local moisture retention, though their statistical representativeness remains limited [19]. Overall, combining these approaches can reduce technique-specific constraints and improve predictions of unsaturated flow behavior in cementitious materials [20].

Building on these classical findings, more recent research has introduced refined experimental approaches and broader comparative analyses, providing further insights into the relationship between pore structure characterization and water retention behavior in cementitious materials. Xiong et al. [21] compared pore size distributions derived from MIP and low-field NMR in UHPC, demonstrating the advantages of NMR in detecting micropores and in capturing dynamic water absorption processes, thereby underlining the complementarity of different techniques. Rodríguez-Brito et al. [22] demonstrated that dynamic water vapor sorption (DWVS) and MIP yield different porosity profiles, underscoring the importance of methodological cross-validation. Abousnina et al. [23] reviewed a wide range of pore measurement techniques – highlighting image analysis as particularly effective for porosity distribution assessment – and emphasized that effective porosity alone cannot reliably predict hydraulic conductivity, unlike total porosity. Additionally, Lamichhane et al. [24] showed how variations in water level and saturation significantly impact both permeability and compressive strength in porous concrete, stressing that moisture-dependent mechanical and hydraulic behavior must be considered when linking microstructural features to unsaturated transport processes. These recent contributions strengthen the framework for interpreting WRC data and highlight the importance of considering methodological aspects and material-specific characteristics in water retention studies.

Combining these techniques can offer a more comprehensive characterization of concrete's pore network; however, key questions remain: How well do their results correlate? How representative are they for water retention behavior? And how does sample size or heterogeneity influence measurements [25]? To address these questions, this study characterizes the water retention behavior and pore size distribution of concrete through:

1. WRC measurements,
2. MIP,
3. CT imaging,
4. SEM analysis.

Special emphasis is placed on evaluating cross-method correlations, assessing the representativeness of measured parameters, and quantifying the influence of sample size. By linking microstructural features to moisture retention behavior, the study aims to provide a more robust foundation for modeling unsaturated water transport in concrete.

2 Materials and methods

2.1 Concrete mixtures and specimen preparation

For the laboratory investigations, two concrete mixtures were prepared with water-to-cement (w/c) ratios of 0.40 and 0.50. The binder was Lafarge CEM II/A-S 42.5 R, a rapid-hardening Portland composite cement incorporating ground granulated blast-furnace slag, with a characteristic compressive strength of 42.5 MPa. The cement content was fixed at 360 kg/m^3.

The aggregate system was comprised of washed, size-fractionated, and oven-dried natural sand and gravelly sand. The proportions were 40% 0/4 mm sand, 25% 4/8 mm coarse sand, and 35% 8/16 mm gravel. The grain size distribution of the aggregate is shown in Fig. 1.

To achieve the desired workability and flow characteristics, a high-range water-reducing admixture based on polycarboxylate ether (PCE), specifically Sika ViscoCrete 4025 Ultra, was incorporated into the mixes as additive. The detailed composition of the concrete mixtures is presented in Table 1.

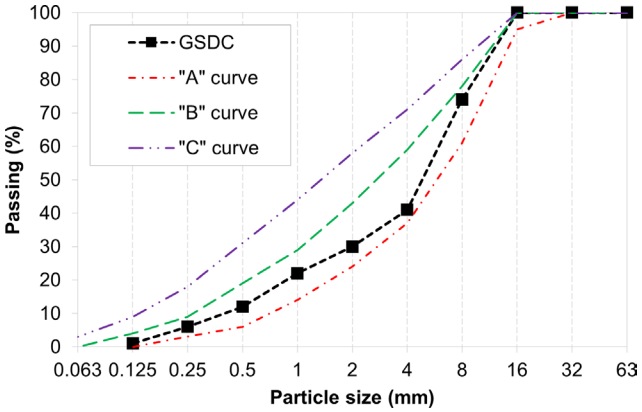

Fig. 1 Grain size distribution of the aggregate used in the concrete mixtures

Table 1 Summary of concrete mixtures tested

Mix No.	Cement type	Cement content (kg/m³)	w/c ratio	PCE content (kg/m³)
C1	CEM II/A-S 42.5 R	360	0.50	1.08
C2	CEM II/A-S 42.5 R	360	0.40	3.60

Concrete mixtures were cast into 150 × 150 × 150 mm cubic molds. From the hardened cubes, cylindrical core samples with a nominal diameter of 50 ± 1 mm were extracted using a diamond-tipped coring drill. For X-ray CT analysis, the cores were sectioned into individual specimens with a nominal height of 50 ± 3 mm using a precision concrete saw (Fig. 2).

Following CT scanning, each core was further processed to obtain one specimen per mixture for WRC measurements. These samples had a diameter of 35 ± 1 mm and a thickness of 5 ± 1 mm (Fig. 3). For SEM and MIP, the required small-volume specimens were obtained by fracturing segments of the original cylindrical cores.

Fig. 2 Concrete specimen prepared for X-ray CT analysis

Fig. 3 Concrete specimen prepared for WRC measurement

All concrete specimens were subjected to a combined curing regime. After demolding, the samples were immersed in lime-saturated water at a temperature of 20 ± 2 °C for 7 days. This was followed by storage under laboratory conditions (22 ± 2 °C, relative humidity ≥ 55%) until testing. All measurements were performed after the specimens reached an age of at least 100 days, ensuring an advanced degree of cement hydration and minimizing the influence of early-age microstructural changes on the test results [26].

2.2 Basic physical properties

At the age of 100 days, the hardened concrete properties were determined, including dry density, compressive strength, total water-accessible porosity, water penetration depth under pressure, and saturated water permeability. These parameters provide essential context for interpreting the subsequent microstructural and hydraulic measurements.

Three specimens were tested per mixture for compressive strength and water penetration depth, while two specimens per mixture were tested for dry density and porosity. Mean values and standard deviations were calculated and reported. Saturated water permeability was determined on a single specimen per mixture using a constant head test in a triaxial cell under a confining pressure of 600 kPa. The permeability test specimens were 50 mm in diameter and 50 mm in height.

In addition, the material density of the concrete samples was measured using gas pycnometer to support the interpretation of porosity data.

The fundamental physical and mechanical properties, along with their respective ranges, for the tested concrete mixtures are summarized in Table 2.

2.3 Experimental techniques

2.3.1 WRC measurement

WRC were determined using a WP4C instrument (Fig. 4), which employs a chilled-mirror dewpoint technique to measure the water potential of porous materials [27]. In this

Table 2 Fundamental properties of concrete mixtures

Physical properties	C1	C2
Dry state density (kg/m³)	2243 ± 17	2313 ± 14
Material density (kg/m³)	2622 ± 1	2619 ± 1
Compressive strength at 100 days (MPa)	60.6 ± 2.1	85.3 ± 0.8
Water-accessible porosity (vol.%)	8.95 ± 0.9	7.09 ± 0.2
Water penetration depth (mm)	21 ± 2.5	10 ± 1.5
Saturated permeability (m/s)	1.19×10^{-10}	7.83×10^{-11}

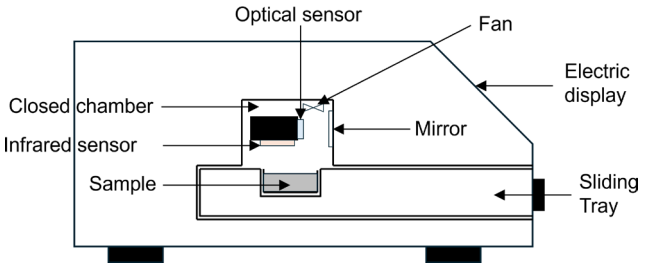

Fig. 4 WP4C device for determining the water potential of concrete specimens

system, the sample equilibrates with the air in a sealed chamber; the mirror's temperature at which condensation first forms indicate the water potential. A thermoelectric cooling system and photoelectric detection are used to determine the dewpoint temperature with high precision.

The sample holder has a total volume of 15 cm^3, with an optimal volume of 7 cm^3 recommended by the manufacturer. Accordingly, disc-shaped specimens with a diameter of 35 ± 1 mm and a height of 5 ± 1 mm were prepared using a diamond core drill and a precision saw. One specimen was tested for each concrete mixture.

Prior to the measurement series, the instrument was calibrated using a calcium chloride solution (0.50 mol/kg), and daily validation was performed with a sodium chloride solution (2.33 mol/kg). Sample saturation was achieved through capillary uptake. Controlled drying steps were defined based on gravimetric mass changes, yielding approximately 10–15 measurement points per sample and covering a suction range from 100 kPa to 300 000 kPa.

After each drying step, specimens were placed in airtight containers for 24 h to allow for internal moisture redistribution. Measurement duration per point ranged from 15 to 60 min, depending on saturation. Specimen masses were recorded using an analytical balance with 0.1 mg precision (Sartorius Entris 121i-1S, Sartorius, Göttingen, Germany). Upon completion of all measurements, samples were oven-dried at 60 ± 5 °C for 24 h to determine the residual water content.

All WP4C measurements were performed in the Soil Mechanics Laboratory of the Department of Engineering Geology and Geotechnics at the Budapest University of Technology and Economics, in accordance with ASTM D6836-25 standard [28].

Numerous empirical models with closed-form equations have been proposed in the literature to represent WRCs [1–3]. The use of such fitted functions not only enhances the comparability of curves obtained from different studies but also improves their applicability in numerical simulations and predictive modelling.

In this study, the measured data points were normalized with respect to the saturated water content. Accordingly, the plotted values and fitted models are expressed in terms of the degree of saturation. Curve fitting was performed using the Fredlund and Xing [3] model, which offers enhanced flexibility for representing the full suction range and, for concrete, has been shown to provide a better fit compared to the van Genuchten model [2]. This model includes an additional correction factor, enabling improved accuracy in the high-suction range.

The Fredlund–Xing model is defined as follows:

$$S_r(\psi) = C(\psi) \times \frac{1}{\left\{ \ln\left[e + \left(\frac{\psi}{\alpha_f} \right)^{n_f} \right] \right\}^{m_f}}, \tag{1}$$

where $S_r(\psi)$ is the degree of saturation of the soil at a given suction, α_f is the fitting parameter related to the air-entry suction (kPa), n_f is the fitting parameter controlling the slope of the transition zone, m_f is the fitting parameter associated with the high suction range, and e is Euler's number. The correction factor can be expressed in the following form:

$$C(\psi) = 1 - \frac{\ln\left(1 + \left[\frac{\psi}{\psi_r} \right] \right)}{\ln\left(1 + \left[\frac{10^6}{\psi_r} \right] \right)}, \tag{2}$$

where ψ_r is the suction value corresponding to the residual saturation (kPa), which was set to a constant value of 10^6 kPa based on the characteristics of concrete and in order to preserve the physical interpretability of the parameter. The WRCs were fitted using the least squares method, aiming to minimize the sum of squared errors between the measured and computed degrees of saturation. The fitting procedure was performed using the Solver add-in of Microsoft Excel [29].

2.3.2 Mercury intrusion porosimetry (MIP)

MIP is one of the most widely used techniques for characterizing the pore structure of porous materials [30]. The method relies on the fact that mercury is a non-wetting liquid for most solids and can only enter pores under external pressure. The required pressure is inversely proportional to the pore diameter. This enables MIP to provide detailed information on pore size distribution, pore volume, and capillary structure characteristics.

In a typical MIP analysis, a specimen with a volume of approximately 1 cm^3 is placed in a vacuum chamber. Mercury is introduced into the chamber, and pressure is gradually increased while the intruded volume is continuously recorded [31]. One of the main advantages of this technique is its wide measurement range – from a few nanometers up to several hundred micrometers – combined with its relatively fast operation and quantitative output [32].

Nevertheless, the method is subject to several well-documented limitations [12, 33]. High intrusion pressures may compress or damage delicate pore structures, while irregular or complex geometries can cause inaccuracies in the interpretation of pore sizes. Furthermore, the detection of very large pores is constrained by mercury's low surface tension, as such pores tend to fill at low pressures, thereby limiting resolution at the coarser end of the pore size spectrum.

MIP tests were performed on two concrete mixtures. The experiments were conducted using a POREMASTER 60 GT MIP (Quantachrome Instruments, Boynton Beach, FL, USA) at the laboratory of SZIKKTI Kft. Pore diameters were calculated assuming a contact angle of 140° and a surface tension of 0.484 N/m based on Eq. (3) [34]:

$$d = \frac{4F\cos\alpha}{P}, \tag{3}$$

where P is the mercury intrusion pressure (Pa), F is the mercury surface tension (N/m), α is the contact angle (°), d is the pore diameter (m).

The effective measurement range of the device was from 950 µm to 3.6 nm. Prior to testing, all specimens were dried at 60 ± 5 °C for 24 h.

2.3.3 X-ray computed tomography (CT)

X-ray CT is a widely used non-destructive imaging technique that enables three-dimensional analysis of internal structures. It is particularly effective for visualizing cracks, voids, and aggregate distribution in cementitious materials, which are critical parameters for assessing durability and hydraulic behavior [15, 35, 36].

CT scanning involves irradiating the specimen from multiple angles, with detectors capturing the transmitted X-rays. The recorded absorption profiles are processed *via* reconstruction algorithms to produce two-dimensional grayscale cross-sections, which can then be compiled into a three-dimensional model of the object [37]. The spatial resolution is determined by the pixel size and slice thickness, and is inherently limited by the physical characteristics of the scanning system [38].

In this study, CT analyses were performed on one concrete specimen from each mixture, which were later also used for WRC measurements. The scans were carried out at the Department of Medical Imaging, Clinical Centre, University of Pécs. Imaging was conducted using a Siemens Somatom Perspective CT scanner, with acquisition parameters optimized for the analysis of construction materials:

- Pixel size: 0.08 × 0.08 mm
- Slice thickness: 0.60 mm
- Resulting voxel resolution: 0.08 × 0.08 × 0.60 mm

Due to this resolution limit, pores smaller than approximately 80 µm could not be reliably detected [38]. Image processing was performed using the open-source software ImageJ [39] to determine pore size and spatial distribution, thereby supporting the interpretation of water transport mechanisms in the concrete. The contrast and brightness settings of the 8-bit images were calibrated using a reference sample, and these settings were then applied consistently to all images to ensure uniform segmentation (Fig. 5). Pores (dark regions) and the solid phase (light regions) were separated through binarization using Otsu's thresholding method [40]. This algorithm yielded more consistent and accurate segmentation results compared to other commonly used methods [41]. For evaluation purposes, the colors in the binarized images were inverted. The processed image slices were then reconstructed into a 3D sample using a trilinear interpolation method.

For each slice, the pore area was calculated as a ratio of the total cross-sectional area. The average porosity of each specimen was then obtained by averaging the values from all slices. The pore size distribution was calculated and evaluated using MATLAB [42] and Microsoft Excel [29] software. For each pore, the equivalent circular diameter (ECD) was determined from the measured cross-sectional pore area and used in subsequent statistical and comparative analyses.

2.3.4 Scanning electron microscopy (SEM)

SEM is a widely used technique in materials science, offering high-resolution imaging of surface morphology

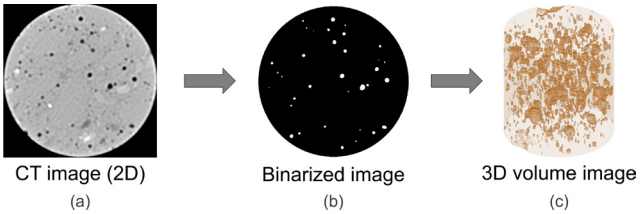

Fig. 5 Workflow of CT image processing: (a) Original grayscale cross-sectional CT image; (b) Binarized image after segmentation using Otsu's thresholding; (c) 3D reconstruction of the pore network

and microstructural features. In the context of cementitious materials, SEM enables the detailed examination of hydration products, microcracks, ITZ, and aggregate–matrix interactions – key parameters for assessing durability and mechanical performance [15, 43].

In this study, SEM analyses were performed on one specimen from each concrete mixture. The samples, approximately 1.0–1.5 cm in diameter, were prepared by fracturing fragments from previously tested specimens. Due to the non-conductive nature of concrete, a thin layer of gold was applied to the samples using sputter coating to prevent surface charging during scanning.

The SEM investigations were conducted using a Phenom XL G2 SEM (Thermo Fischer Scientific, Waltham, MA, USA) at the Department of Construction Materials and Technologies, Budapest University of Technology and Economics.

SEM image processing was performed using ImageJ software [39]. The processing steps – noise removal, image quality enhancement, regularization, binarization, and thresholding (Otsu method) – followed the procedures described by Andrushia et al. [41] and Li et al. [44]. In binarized images, black regions typically represent pores, and light regions correspond to the solid phase; however, for evaluation purposes, the colors were inverted (Fig. 6).

The pore size distribution of the specimens was computed and analyzed with MATLAB [42] and Microsoft Excel [29] software. The samples and their pore distributions were examined at magnifications of 500×, 1000×, and 2500×. For each magnification, a single image was analyzed, with higher magnifications focusing on a subregion of the previously investigated area. The ECD was used for the analysis, following the same approach applied in the CT evaluation.

3 Results and discussion

3.1 Water retention behavior

The Fredlund and Xing parameters obtained from curve fitting are presented in Table 3, while the measured data

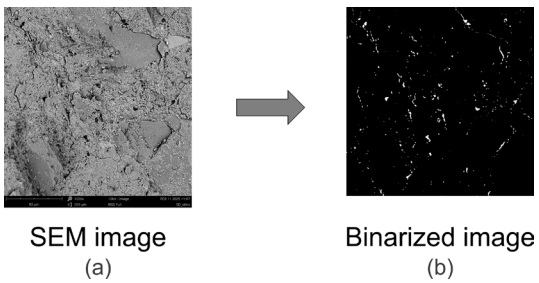

Fig. 6 Workflow of SEM image processing: (a) Original high-magnification SEM micrograph of the concrete surface; (b) Binarized image after segmentation for pore identification

Table 3 Fredlund–Xing model fitting parameters and sum of squared errors (SSE) for the drying WRCs

Mix. No.	α_f (kPa)	n_f	m_f	SSE
C1	69323	0.6352	5.0893	7.77×10^{-3}
C2	43146	0.6955	3.9478	1.25×10^{-2}

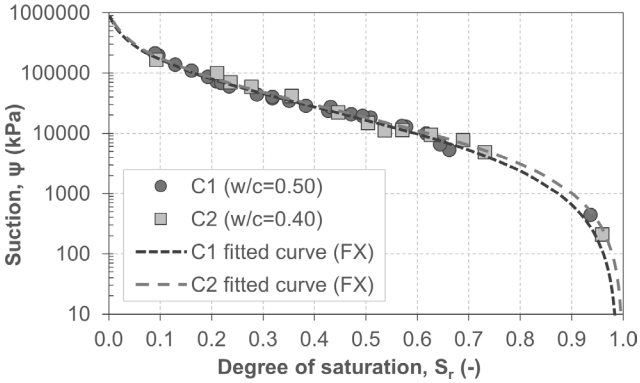

Fig. 7 Drying WRCs for concrete mixtures tested

points and the fitted curves are illustrated in Fig. 7.

The curves clearly indicate an air entry value of approximately 1000 kPa. Depending on the concrete quality (i.e., pore size distribution), the residual zone is reached at a suction value of approximately 200 000 kPa, with varying slopes. Despite similar overall characteristics, it is evident that variations in pore size distribution influence the slope of the WRC in the transition zone, which in turn can significantly affect the unsaturated hydraulic conductivity.

To quantitatively characterize the slope of the WRC, the substitute equation of Fredlund and Xing model was applied [45]. This equation is based on the relationship between the degree of saturation and the exponent of the base 10 logarithm of suction. When plotted in an arithmetic coordinate system, the substitute curve reproduces the same shape as the original WRC; consequently, its inflection point, and the slope of the tangent fitted at that point are identical to those of the original curve. The general form of the substitute equation can be expressed as follows:

$$S_r(\zeta) = \frac{1 - \ln\left(1 + \frac{10^{\zeta}}{\psi_r}\right)}{\ln\left(1 + \frac{10^{6}}{\psi_r}\right)} \Bigg/ \left\{\ln\left[e + \left(\frac{10^{\zeta}}{\alpha_f}\right)^{n_f}\right]\right\}^{m_f}, \tag{4}$$

where ζ is $\log_{10}(\psi)$, $S_r(\zeta)$ is the degree of saturation at given suction, and ψ is the suction (kPa).

The coordinates of the inflection point, and the slope of the tangent were determined using an extremum search method based on the first and second derivatives of the

substitution function. The calculations were performed using MATLAB software [42]. For each concrete mix, the location of the inflection point $\{\zeta_{inf}, S_r(\zeta_{inf})\}$, the corresponding suction value $\{\psi_{inf}\}$, and the slope of the curve at that point $\{S_r'(\zeta_{inf})\}$ are summarized in Table 4.

The w/c ratios were 0.40 and 0.50, with corresponding slope values of −0.4865 and −0.4672, respectively. Based on these results, there appears to be a tendency for a higher w/c ratio to correspond to a lower absolute slope value, suggesting that the curve becomes flatter as the w/c ratio increases. Such flattening of the WRC may indicate a broader pore size distribution, which in this context could imply a higher proportion of larger diameter pores within the concrete. Factors that are likely to increase the amount or size of pores in the concrete would be expected to contribute to this flattening.

3.2 Evaluation of pore size distribution from MIP

MIP measurements were conducted to characterize the pore structure of concrete within a pore diameter range of 195.5 μm to 3.6 nm. The results are presented in Table 5. For both concrete types investigated, the most frequent pore size range was between 5.1 nm and 37.4 nm. In the concrete with a w/c ratio of 0.50, a narrower dominant pore size distribution was observed. Overall, the mix with a 0.40 w/c ratio exhibited lower total porosity than the mix with a 0.50 ratio.

It should be noted that the sample size used for the MIP tests was small relative to the macroscopic heterogeneity of concrete. Therefore, the results may not fully represent the overall pore size distribution of the material. In addition, the specimens did not contain aggregate particles, meaning that the measured porosity reflects only the cement paste and not the ITZ [12, 19].

Furthermore, mercury can only intrude into open pores – that is, those connected to the external surface and the capillary network, through which fluid transport is possible. Consequently, the porosity determined *via* MIP in the investigated pore diameter range should be regarded as the apparent porosity of the sample.

Figs. 8 and 9 present the pore diameter frequency based on pore volume and the variation of porosity as a function of pore diameter, respectively.

The pore size distribution and frequency exhibit similar overall trends for both samples; however, noticeable differences are observed in the total pore volume and the distribution across specific pore size ranges. The concrete with a 0.40 w/c ratio contains a higher number of smaller pores, while the 0.50 mix shows a greater proportion of larger pores in comparison.

Table 4 Quantitative analysis of the slope of drying WRCs

Inflection point data	C1	C2
ζ_{inf} $\{S_r''(\zeta)=0\}$	4.4102	4.3937
ψ_{inf} (kPa)	25716	24757
$S_r(\zeta_{inf})$	0.4168	0.4356
$S_r'(\zeta_{inf})$	−0.4672	−0.4865

Table 5 Results of MIP experiments

Mix. No.	Pore diameter range	Most frequent pore diameter	Cumulative pore volume (cm³/g)	MIP porosity (vol.%)
C1	0.0036–195.5 μm	11.1–18.5 nm	0.0249	6.03
C2	0.0036–190.6 μm	5.1–37.4 nm	0.0157	3.89

3.3 Estimation of WRC from MIP data

Understanding WRCs is essential for investigating and modeling water movement in concrete. However, their determination using conventional methods is often highly time-consuming.

As mentioned on several occasions, WRCs can essentially be regarded as representations of the pore size distribution, and they are also closely related to the hydraulic

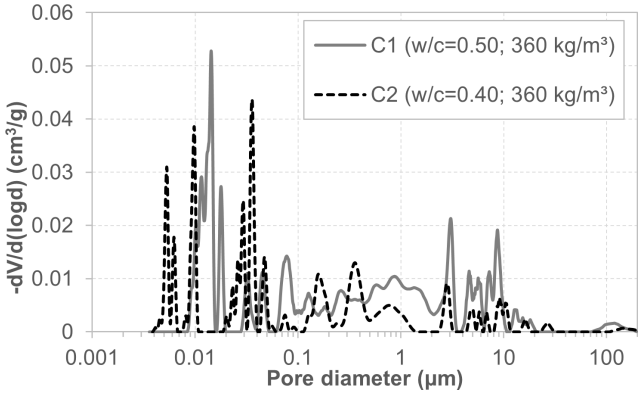

Fig. 8 Differential pore size distribution curves obtained from MIP for concrete mixtures tested

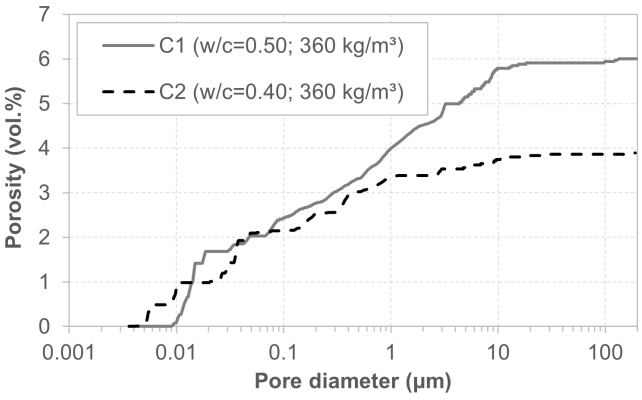

Fig. 9 Cumulative pore size distribution curves obtained from MIP for concrete mixtures tested

conductivity function [46]. The inverse application of the Barrett–Joyner–Halenda (BJH) method [47] may provide a reliable methodological basis for deriving the WRC from pore size distribution data.

The BJH method was originally developed for the interpretation of adsorption isotherms; however, in its inverse form, it can also be applied to determine the WRC. The pore sizes determined by MIP can be converted into suction values based on capillary pressure, using a rearranged form of the capillary equation (Eq. (3)), as follows:

$$\psi = \frac{4F\cos\alpha}{d}, \tag{5}$$

where ψ is the suction (kPa), F is the surface tension of water at laboratory temperature (~0.072 kN/m), α is the contact angle (0°), and d is the pore diameter (m). Based on the saturation calculated from the pore size distribution, the WRC can then be approximated and fitted.

MIP often underestimates the actual water retention, as mercury may not penetrate the smallest pore entrances due to complex pore geometries – although these pores are still capable of storing water [12]. This method primarily captures the pore domain associated with capillary water.

The BJH procedure assumes cylindrical pore geometry, which does not always apply to concrete or cement paste [4]. The application of the BJH method to MIP data – due to the non-wetting nature of mercury – is mainly suitable for approximating the drying branch of the WRC. The method yields reliable approximations in the 0.002–0.050 μm pore size range, corresponding approximately to a suction range of 5000–150000 kPa. According to the results of Zhang et al. [48], permeability and water transport are primarily governed by pores in the 0.010–1 μm size range, which is in good agreement with the measurement range typically covered by MIP, spanning approximately 0.003 to 200 μm.

Since the goal was to develop a fast and practical approximation method, the thickness of the adsorbed water film, which would reduce the effective pore radius, was neglected. This effect is mainly relevant in the fine pore size range and can be estimated using, for example, the BET method [4, 49].

Figs. 10 and 11 compare the WRCs measured and calculated from the MIP data. In both cases the curves were fitted using the Fredlund and Xing model. The fitting parameters used are listed in Table 6. For the parameter α_f, an upper limit of 100 000 kPa was applied to ensure physical plausibility.

The characteristics of the calculated and fitted curves are generally similar; however, they tend to underestimate the actual water retention capacity of the concrete. In the case of the C2 concrete mix, the estimated curve provides a close approximation to the experimentally measured drying branch of the WRC.

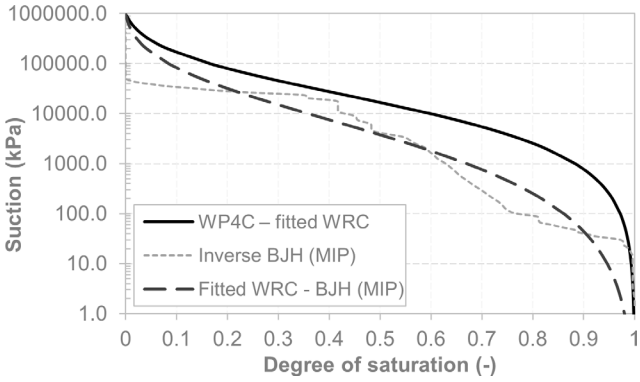

Fig. 10 Comparison of WRCs for C1 mixture obtained from WP4C measurements (fitted WRC) and those derived from MIP data using the inverse BJH method, including the fitted WRC based on BJH-derived data

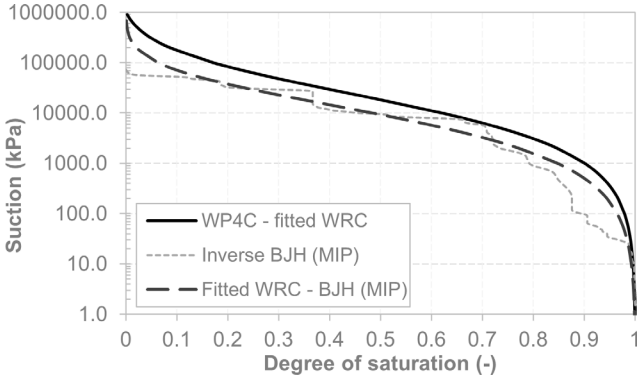

Fig. 11 Comparison of WRCs for C2 mixture obtained from WP4C measurements (fitted WRC) and those derived from MIP data using the inverse BJH method, including the fitted WRC based on BJH-derived data

Table 6 WRC fitting parameters from inverse BJH method and sum of squared errors

Mix. No.	α_f (kPa)	n_f	m_f	SSE
C1	100000	0.4377	8.5326	5.509
C2	100000	0.6627	9.5981	2.985

Nevertheless, at the current stage of the research, the method should be considered only as a rough approximation. The findings also highlight that, due to the small size of the specimens analyzed in the MIP tests, the resulting data may not adequately represent the full pore size distribution – and consequently the water retention characteristics – of the entire concrete matrix.

3.4 CT and SEM image analysis

The diameters of pores identified *via* CT scanning ranged from 95 to 6480 μm, and thus the calculated porosity values represent the proportion of pores within this size range. It is important to note that the upper limit of 6480 μm does not reflect a technical limitation of the CT

method but rather corresponds to the largest pore detected. The CT-derived porosity was 1.91% for the concrete with a 0.40 w/c ratio, and 3.36% for the mix with 0.50.

In contrast, SEM analysis identified significantly smaller pores, ranging from 0.11 to 21.21 μm. Although the magnification level had minimal impact on the detectable pore size range, it clearly influenced the calculated porosity, as reported by [41]. This effect is likely due to the fact that higher magnifications allow finer features to be resolved during image processing, resulting in a greater proportion of pores being detected and, consequently, higher porosity values (Fig. 12).

Since only a narrow range of pore sizes could typically be detected at 1000× SEM magnification, the resulting porosity values were lower than the total and apparent porosity values obtained from other methods. Additionally, for the C2 concrete mix (w/c = 0.40), a higher porosity value was observed compared to the C1 mix (Table 7).

Total porosity was calculated based on the measured dry density and material density. This value includes all pores, including closed pores that do not contribute to water transport. As expected, total porosity is significantly higher than the porosity values determined by MIP, CT, or SEM, highlighting that these techniques, when used individually, are insufficient to capture the full pore volume.

MIP and CT cover a wide range of pore sizes – from 3.6 nm to 6.5 mm – and the sum of the porosities obtained from these methods most closely approximates the volume of water-accessible pores. However, it is essential to note that there is an overlap in the measurable pore size ranges of the two methods, which may lead to partial double-counting.

Moreover, CT provides total porosity within its resolution limits, including both connected and isolated pores visible at the macroscopic scale, whereas MIP measures only the volume of open and connected pores, primarily in the micro- and mesopore range.

The Weibull and lognormal distributions were applied to describe pore size distributions, which are widely used in materials science [50]. The lognormal distribution is suitable when pore sizes exhibit an asymmetric distribution and take only positive values. The Weibull distribution effectively characterizes the shape of the distribution curve, especially when pore sizes are concentrated within a specific range.

Figs. 13 and 14 show the pore size distribution of the tested concrete mixtures. The measured data exhibit a right-skewed distribution, with the lognormal model providing a closer fit to the experimental values across the full pore size range. Based on the sum of squared errors (SSE), the lognormal distribution better approximates the pore size distributions obtained from both CT and SEM analyses (Table 8).

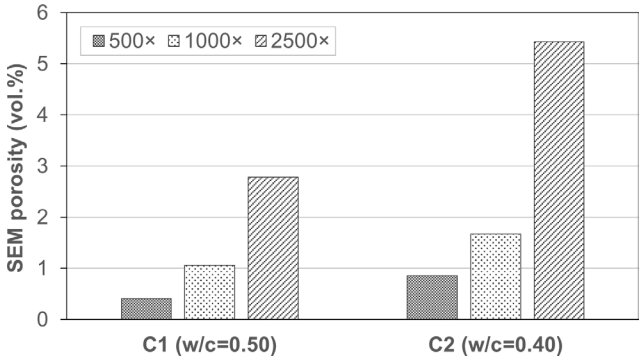

Fig. 12 SEM-based porosity of concretes C1 (w/c = 0.50) and C2 (w/c = 0.40) at different magnifications (500×, 1000×, and 2500×)

Table 7 Comparison of porosity values obtained using different measurement techniques (vol.%)

Mix. No.	Total porosity	MIP porosity	CT porosity	SEM porosity (1000×)	Water-accessible porosity
C1	14.00	6.03	3.36	1.06	8.95
C2	12.07	3.89	1.91	1.67	7.09

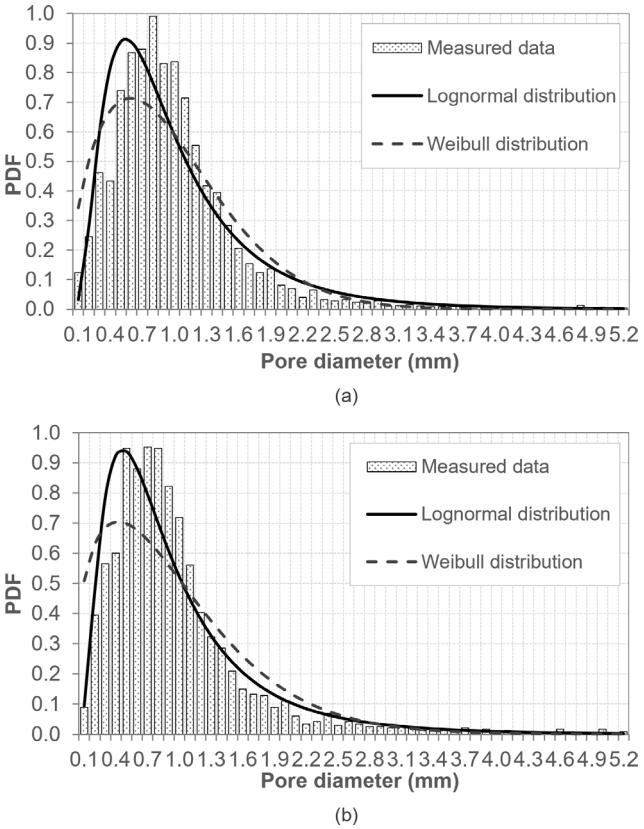

Fig. 13 Pore size distribution from CT analysis fitted with lognormal and Weibull models: (a) C1 mixture (w/c = 0.50); (b) C2 mixture (w/c = 0.40)

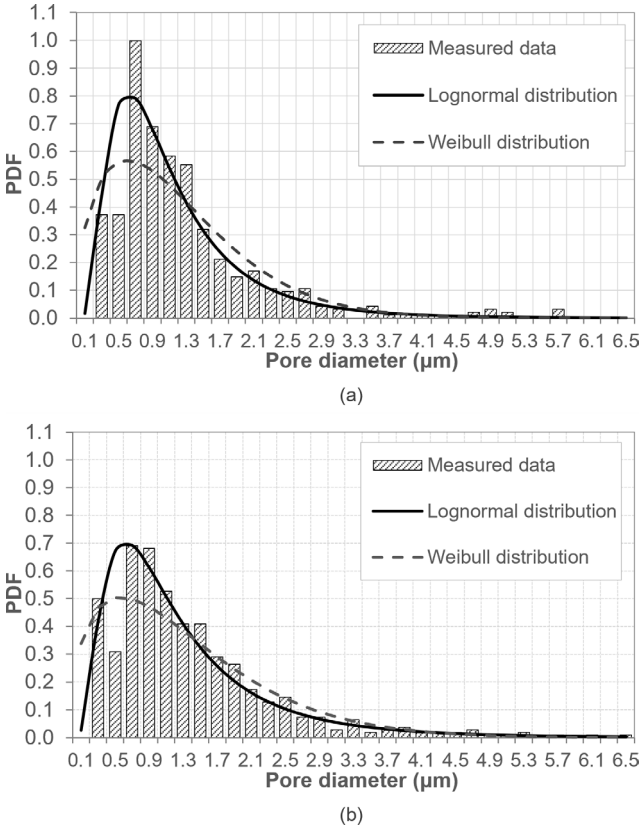

Fig. 14 Pore size distribution from SEM analysis fitted with lognormal and Weibull models: (a) C1 mixture (w/c = 0.50); (b) C2 mixture (w/c = 0.40)

Table 8 Least square errors for each measurement method

Mix. No.	Measurement	Lognormal	Weibull
C1	CT	0.428	0.520
	SEM	0.235	0.426
C2	CT	0.362	0.756
	SEM	0.160	0.258

4 Conclusions

Using multiple analytical techniques, this study investigated the water retention behavior and pore size distributions of two concrete mixtures with different w/c ratios. The WRC was measured using the WP4C device, while porosity characteristics were examined through MIP, X-ray CT, and SEM. The key conclusions are as follows:

- The mixture with a w/c ratio of 0.40 exhibited a higher number of finer pores, while the 0.50 w/c mixture contained a greater proportion of larger pores, resulting in a broader pore size distribution. These differences were clearly reflected in the shape of the WRCs, where the flatter slope in the transition zone of the higher w/c ratio mixture indicates increased sensitivity of hydraulic conductivity to changes in suction. Such differences have direct implications for the durability and watertightness of concrete used in deep foundations and containment structures.
- The WRC could be estimated from MIP-based pore size distributions using the inverse BJH method, providing a useful rapid approximation. However, the method systematically underestimated retention values because mercury cannot penetrate all pore domains, particularly the finest ones. Therefore, while valuable as a supporting tool, MIP-based estimation cannot replace direct WRC measurement when reliable hydraulic characterization is required.
- SEM analysis provided high-resolution insights into microstructural features and smaller pores, but the limited field of view and sensitivity to magnification strongly influenced the calculated porosity values. In addition, not all dark features in binarized SEM images necessarily represent true pores. As a result, SEM is more suitable for qualitative or comparative pore analysis than for quantitative determination of total porosity.
- CT scanning effectively captured the distribution of larger pores and allowed visualization of macroscopic heterogeneity in the specimens. However, due to its resolution threshold, micropores could not be reliably detected, which means CT alone cannot fully describe the pore network of cementitious materials.
- Pore size distributions obtained from both CT and SEM data were better represented by lognormal than Weibull distributions. This suggests that probabilistic modeling of pore structures using lognormal functions can provide a more accurate description for use in hydraulic property estimation and numerical modeling.
- No single technique was sufficient to capture the full range of pore sizes or to represent water retention behavior on its own. MIP and CT together cover a wide pore size spectrum and, when used in combination, can approximate the water-accessible porosity more closely. However, overlapping detection ranges and differences in the types of pores detected must be carefully considered to avoid misinterpretation.

Further work should refine the indirect estimation of WRCs from pore structure data, with improved calibration of MIP-based methods. Multi-method integration should be validated on larger and more heterogeneous specimens to address scale effects. Studies on concretes with alternative binders or supplementary cementitious materials would improve generalizability. Advanced techniques

such as micro-CT, combined with digital image analysis and numerical simulations, could better link pore structure to hydraulic behavior, supporting more reliable predictions of unsaturated transport properties and the design of durable, watertight infrastructure.

Acknowledgement

The project presented in this article is supported by the EKOP-24-4-I-157 University Research Scholarship Program of the Ministry for Culture and Innovation from the source of the National Research, Development and Innovation fund.

References

[1] Mualem, Y. "A new model for predicting the hydraulic conductivity of unsaturated porous media", Water Resources Research, 12(3), pp. 513–522, 1976
https://doi.org/10.1029/WR012i003p00513

[2] van Genuchten, M. T. "A Closed-form Equation for Predicting the Hydraulic Conductivity of Unsaturated Soils", Soil Science Society of America Journal, 44(5), pp. 892–898, 1980.
https://doi.org/10.2136/sssaj1980.03615995004400050002x

[3] Fredlund, D. G., Xing, A. "Equations for the soil-water characteristic curve", Canadian Geotechnical Journal, 31(4), pp. 521–532, 1994.
https://doi.org/10.1139/t94-061

[4] Leech, C. A. "Water Movement in Unsaturated Concrete: Theory, Experiments, Models", PhD Thesis, School of Engineering, The University of Queensland, 2003.
https://doi.org/10.14264/157970

[5] Major, J., Wittmann, F. H., Sadouki, H. "Drying and Hygral Diffusion Coefficient of Concrete", Restoration of Buildings and Monuments, 16(1), pp. 39–46, 2010.

[6] Pap, M., Mahler, A., Nehme, S. G. "Analysis and Finite Element Modelling of Water Flow in Concrete", Periodica Polytechnica Civil Engineering, 62(4), pp. 1052–1059, 2018.
https://doi.org/10.3311/PPci.13005

[7] Törzs, T., Lu, G., Monteiro, A. O., Wang, D., Grabe, J., Oeser, M. "Hydraulic properties of polyurethane-bound permeable pavement materials considering unsaturated flow", Construction and Building Materials, 212, pp. 422–430, 2019.
https://doi.org/10.1016/j.conbuildmat.2019.03.201

[8] Park, K., Fleming, I. R. "Evaluation of a geosynthetic capillary barrier", Geotextiles and Geomembranes, 24(1), pp. 64–71, 2006.
https://doi.org/10.1016/j.geotexmem.2005.06.001

[9] Chaparro, M. C., Saaltink, M. W. "Water, vapour and heat transport in concrete cells for storing radioactive waste", Advances in Water Resources, 94, pp. 120–130, 2016.
https://doi.org/10.1016/j.advwatres.2016.05.004

[10] Huynh, T.-P., Ngo, S.-H., Nguyen, V.-D. "A Modified Reactive Powder Concrete Made with Fly Ash and River Sand: An Assessment on Engineering Properties and Microstructure", Periodica Polytechnica Civil Engineering, 68(4), pp. 1031–1039, 2024.
https://doi.org/10.3311/PPci.23912

[11] Poornamazian, A., Izadinia, M. "A Comprehensive Investigation of Performance Characteristics, Mechanical Properties and Durability Parameters of Self-compacting Concrete Containing Iron Slag as Coarse Aggregate", Periodica Polytechnica Civil Engineering, 68(2), pp. 498–510, 2024.
https://doi.org/10.3311/PPci.22846

[12] Miao, L., Wen, M., Jiao, C., He, S., Guan, X. "Concrete microstructure characterized by multi-measurement techniques considering fly ash contents and concrete sample sizes", Case Studies in Construction Materials, 20, e03315, 2024.
https://doi.org/10.1016/j.cscm.2024.e03315

[13] Navarrete-Seras, M. A., Alonso-Guzmán, E. M., Martínez-Molina, W., Chávez-García, H. L., Arreola-Sánchez, M., Borrego-Perez, J. A., Cervantes-Servín, A. I. "Finite Element Modeling with Ultrasonic Pulse Velocity for Visualising Rock Deformations", Periodica Polytechnica Civil Engineering, 69(2), pp. 470–481, 2025.
https://doi.org/10.3311/PPci.38644

[14] Chung, S.-Y., Kim, J.-S., Stephan, D., Han, T.-S. "Overview of the use of micro-computed tomography (micro-CT) to investigate the relation between the material characteristics and properties of cement-based materials", Construction and Building Materials, 229, 116843, 2019.
https://doi.org/10.1016/j.conbuildmat.2019.116843

[15] Abdelmelek, N., Lublóy, É. "Effects of Elevated Temperatures on the Properties of High Strength Cement Paste Containing Silica Fume", Periodica Polytechnica Civil Engineering, 66(1), pp. 127–137, 2022.
https://doi.org/10.3311/PPci.17549

[16] Gallé, C. "Effect of drying on cement-based materials pore structure as identified by mercury intrusion porosimetry: A comparative study between oven-, vacuum-, and freeze-drying", Cement and Concrete Research, 31(10), pp. 1467–1477, 2001.
https://doi.org/10.1016/S0008-8846(01)00594-4

[17] Promentilla, M. A. B., Sugiyama, T., Hitomi, T., Takeda, N. "Quantification of tortuosity in hardened cement pastes using synchrotron-based X-ray computed tomography", Cement and Concrete Research, 39(6), pp. 548–557, 2009.
https://doi.org/10.1016/j.cemconres.2009.03.005

[18] Landis, E. N., Keane, D. T. "X-ray microtomography", Materials Characterization, 61(12), pp. 1305–1316, 2010.
https://doi.org/10.1016/j.matchar.2010.09.012

[19] Scrivener, K. L., Crumbie, A. K., Laugesen, P. "The Interfacial Transition Zone (ITZ) Between Cement Paste and Aggregate in Concrete", Interface Science, 12(4), pp. 411–421, 2004.
https://doi.org/10.1023/B:INTS.0000042339.92990.4c

[20] Roels, S., Carmeliet, J. "Analysis of moisture flow in porous materials using microfocus X-ray radiography", International Journal of Heat and Mass Transfer, 49(25–26), pp. 4762–4772, 2006.
https://doi.org/10.1016/j.ijheatmasstransfer.2006.06.035

[21] Xiong, X.-R., Wang, J.-Y., She, A.-M., Lin, J.-M. "Characterization of Pore Size Distribution and Water Transport of UHPC Using Low-Field NMR and MIP", Materials, 16(7), 2781, 2023.
https://doi.org/10.3390/ma16072781

[22] Rodríguez-Brito, N., Blanco-Peñalver, C., Souto, R. M., Andrade, C., Santana, J. J. "Reassessment of Porosimetry Determinations Using Water Vapor Sorption Measurements for Pastes and Concretes Containing Basaltic Aggregates Compared to the Mercury Intrusion Method", Materials, 18(10), 2257, 2025. https://doi.org/10.3390/ma18102257

[23] Abousnina, R., Aljuaydi, F., Benabed, B., Almabrok, M. H., Vimonsatit, V. "A State-of-the-Art Review on the Influence of Porosity on the Compressive Strength of Porous Concrete for Infrastructure Applications", Buildings, 15(13), 2311, 2025. https://doi.org/10.3390/buildings15132311

[24] Lamichhane, R., Motra, G. B., Khadka, T. B., Zhang, Y. X., Pathak, P., Pandit, S. "Impact of Water Level Variation on Mechanical Properties of Porous Concrete", Sustainability, 16(9), 3546, 2024. https://doi.org/10.3390/su16093546

[25] Czachor, H., Rajkai, K., Lichner, L., Jozefaciuk, G. "Sample geometry affects water retention curve: Simulation and experimental prove", Journal of Hydrology, 588, 125131, 2020. https://doi.org/10.1016/j.jhydrol.2020.125131

[26] Laczkó, L., Wojnárovitsné Hrapka, I., Spránitz, F. "A víz-cement tényező hatása a cementek hidratációjára" (Effect of water/cement ratio on cement hydration), Journal of Silicate Based and Composite Materials, 74(4), pp. 156–162, 2022. (in Hungarian) https://doi.org/10.14382/epitoanyag-jsbcm.2022.24

[27] METER Group Inc. "WP4C Dew Point PotentiaMeter Operator's Manual", [pdf] METER Group Inc., Pullman, WA, USA, 2024. Available at: https://library.metergroup.com/Manuals/20588_WP4C_Manual_Web.pdf [Accessed: 01 September 2024]

[28] ASTM International "ASTM D6836-25 Standard Test Methods for Determination of the Soil Water Characteristic Curve", ASTM International, West Conshohocken, PA, USA, 2025.

[29] Microsoft Corporation "Microsoft Excel, (16.0)", [computer program] Available at: https://office.microsoft.com/excel [Accessed: 22 March 2025]

[30] Diamond, S. "Mercury porosimetry: An inappropriate method for the measurement of pore size distributions in cement-based materials", Cement and Concrete Research, 30(10), pp. 1517–1525, 2000. https://doi.org/10.1016/S0008-8846(00)00370-7

[31] Giesche, H. "Mercury Porosimetry: A General (Practical) Overview", Particle & Particle Systems Characterization, 23(1), pp. 9–19, 2006. https://doi.org/10.1002/ppsc.200601009

[32] Haider, U., Ali, A., Bittnar, Z., Humayon, M., Valentin, J. "Effects of Wet Separated and High Speed Milling Fly Ash Added in High Volume to Cementitious Materials", Periodica Polytechnica Civil Engineering, 64(1), pp. 81–100, 2020. https://doi.org/10.3311/PPci.14846

[33] Çetintaş, S. "Investigation of Pore and Filling Material Bond in Filled Travertine Used as a Building Material", Periodica Polytechnica Civil Engineering, 67(1), pp. 80–92, 2023. https://doi.org/10.3311/PPci.20845

[34] Washburn, E. W. "The Dynamics of Capillary Flow", Physical Review, 17(3), pp. 273–283, 1921. https://doi.org/10.1103/PhysRev.17.273

[35] Dufka, Á., Žižková, N., Brožovský, J. "An Analysis of Crystalline Admixtures in Terms of Their Influence on the Resistance of Cementitious Composites to Aggressive Environments", Periodica Polytechnica Civil Engineering, 65(1), pp. 344–352, 2021. https://doi.org/10.3311/PPci.14514

[36] Csorba, K., Kapitány, K., Cimer, Z., Hlavička, V., Biró, A., Lublóy, É. "Monitoring of historical structural materials with computed tomography", Structural Concrete, 2024. https://doi.org/10.1002/suco.202400149

[37] Lublóy, É., Ambrus, D., Kapitány, K., Barsi, Á. "Air Void Distribution of Asphalts Determined by Computed Tomography", Periodica Polytechnica Civil Engineering, 59(4), pp. 503–510, 2015. https://doi.org/10.3311/PPci.7608

[38] Bossa, N., Chaurand, P., Vicente, J., Borschneck, D., Levard, C., Aguerre-Chariol, O., Rose, J. "Micro- and nano-X-ray computed-tomography: A step forward in the characterization of the pore network of a leached cement paste", Cement and Concrete Research, 67, pp. 138–147, 2015. https://doi.org/10.1016/j.cemconres.2014.08.007

[39] National Institutes of Health "ImageJ, (1.54g)", [computer program] Available at: https://imagej.net/ij [Accessed: 22 March 2025]

[40] Otsu, N. "A Threshold Selection Method from Gray-Level Histograms", IEEE Transactions on Systems, Man, and Cybernetics, 9(1), pp. 62–66, 1979. https://doi.org/10.1109/TSMC.1979.4310076

[41] Andrushia, D. A., Anand, N., Lublóy, É., Naser, M. Z., Kanagaraj, B. "SEM Image-based Porosity Analysis of Fire Damaged High Strength Concrete", Periodica Polytechnica Civil Engineering, 68(2), pp. 559–570, 2024. https://doi.org/10.3311/PPci.22917

[42] The MathWorks, Inc. "MATLAB, (R2024b)", [computer program] Available at: https://www.mathworks.com [Accessed: 15 March 2025]

[43] Dacić, A., Fenyvesi, O., Kopecskó, K. "Investigation of Waste Perlite and Recycled Concrete Powders as Supplementary Cementitious Materials", Periodica Polytechnica Civil Engineering, 67(3), pp. 683–694, 2023. https://doi.org/10.3311/PPci.21593

[44] Li, X., Lin, H., Chen, W., Liang, S., Huang, L. "A numerical study on the tensile splitting of concrete with digital image processing", Journal of Materials Research and Technology, 25, pp. 1626–1641, 2023. https://doi.org/10.1016/j.jmrt.2023.06.026

[45] Zhang, F., Fredlund, D. G. "Examination of the estimation of relative permeability for unsaturated soils", Canadian Geotechnical Journal, 52(12), pp. 2077–2087, 2015. https://doi.org/10.1139/cgj-2015-0043

[46] Rajkai, K., Tóth, B., Barna, G., Hernádi, H., Kocsis, M., Makó, A. "Particle-size and organic matter effects on structure and water retention of soils", Biologia, 70(11), pp. 1456–1461, 2015. https://doi.org/10.1515/biolog-2015-0176

[47] Barrett, E. P., Joyner, L. G., Halenda, P. P. "The Determination of Pore Volume and Area Distributions in Porous Substances. I. Computations from Nitrogen Isotherms", Journal of the American Chemical Society, 73(1), pp. 373–380, 1951.
https://doi.org/10.1021/ja01145a126

[48] Zhang, Y., Xu, S., Fang, Z., Zhang, J., Mao, C. "Permeability of Concrete and Correlation with Microstructure Parameters Determined by ^{1}H NMR", Advances in Materials Science and Engineering, 2020(1), 4969680, 2020.
https://doi.org/10.1155/2020/4969680

[49] Brunauer, S., Emmett, P. H., Teller, E. "Adsorption of Gases in Multimolecular Layers", Journal of the American Chemical Society, 60(2), pp. 309–319, 1938.
https://doi.org/10.1021/ja01269a023

[50] Chung, S.-Y., Sikora, P., Rucinska, T., Stephan, D., Elrahman, M. A. "Comparison of the pore size distributions of concretes with different air-entraining admixture dosages using 2D and 3D imaging approaches", Materials Characterization, 162, 110182, 2020.
https://doi.org/10.1016/j.matchar.2020.110182